ChemComm

COMMUNICATION

View Article Online
View Journal | View Issue

Cite this: *Chem. Commun.*, 2016, 52, 13409

Received 5th October 2016,
Accepted 20th October 2016

DOI: 10.1039/c6cc08047b

www.rsc.org/chemcomm

A simple way to fine tune the redox potentials of cobalt ions encapsulated in nitrogen doped graphene molecular catalysts for the oxygen evolution reaction†

Jiong Wang,[a] Wen-Feng Lin,[b] Yi Shi,[a] Huai-Song Wang,[a] Lian-Qing Rong*[c] and Xing-Hua Xia*[a]

Co^{2+} ions encapsulated in nitrogen doped graphene were applied as an oxygen evolution catalyst. Their redox potentials were tuned using different counter anions as liable ligands, and the redox potential related catalytic rates were explored. It was proposed that the electron density of Co^{2+} ions was a general descriptor for activity.

Combustion of fossil fuels dominates the global energy outputs, but causes the growth of fuel shortage and environmental pollution. One of the promising approaches to address these issues is the production of alternative chemical fuels *via* solar power and electrolysis driven water splitting or artificial photosynthesis.[1–4] Energy conversion in these devices is systematically engineered such that multiple physical and chemical processes, including mass diffusion, and interfacial electron transfer and transport, are integrated into compartmentalized spaces. Among them, electron transfer at heterogeneous interfaces is the rate-determining step. The high efficiency of energy conversion requires fast cathodic and anodic reactions with matching kinetics.[3,5] In particular, the oxygen evolution reaction (OER) is a common anodic reaction, which is however kinetically sluggish.[6,7] The potential required to drive the OER is greater than the standard value (1.23 V *vs.* SHE) for overcoming kinetic barriers. Furthermore, the OER pathways, which involve multiple elemental steps for coupled transfer of electrons and protons, and bonding a pair of oxygen atoms, are highly complicated. It has been reported that different intermediates, known as reactive oxygen species (ROS), are involved in enabling the OER to proceed. Identifying the nature of ROS is important, as they can determine the origin of the overpotential during oxygen conversion.[8] However, to do so is challenging due to the short lifetimes of the intermediates.

First-row transition metal (Co, Ni, *etc.*) based materials have been widely examined as classical OER catalysts.[9–14] It is well accepted that the metal cations exposed at materials' surfaces are mostly responsible for the OER activity.[15,16] Surface metal cations can exhibit different bond strengths with the oxygen intermediates during the OER to affect the overall rate of the catalytic reaction.[17] The significance of metal cations as OER active sites can also be recognized by the type of natural OER catalyst, *i.e.*, the oxygen evolving complex (OEC) of enzyme photosystem II.[18] The geometry of the OEC is a cube framework sustained by a $CaMn_4O_5$ cluster. Catalysis is triggered by the redox active Mn^{2+} ions. Recent reports proposed that the redox properties of Mn^{2+} ions could be tuned by redox-inactive Ca^{2+} ions at the neighboring sites, which is closely related to the origin of the catalytic activity of the OEC.[19,20] These results suggest that high OER activity can be achieved by tuning the surrounding environments of active sites. Although much progress has been achieved, challenges still remain, especially in the aspect of gaining better fundamental principles of catalyst design. To explore the potential of metal cations for OER catalysis, we believe that it is important to further develop appropriate matrices with properties such as high surface area, electrical conductivity and chemical stability, in order to support metal cation based active sites. Furthermore, such catalysts can serve as a framework to probe the descriptor that governs the activity of metal cations.

In this work, we propose a novel and general strategy to synthesize OER electrocatalysts at room temperature simply by immobilizing Co^{2+} ions onto a nitrogen doped graphene (NG) matrix as driven by coordination. The direct connection of Co^{2+} ions to the graphene conductive basal plane combined with the electron tuning ability of conjugated π electrons of graphene is expected to facilitate the heterogeneous electron transfer and transport of redox processes. The resulting electrocatalyst

[a] *State Key Laboratory of Analytical Chemistry for Life Science and Collaborative Innovation Center of Chemistry for Life Sciences, School of Chemistry and Chemical Engineering, Nanjing University, Nanjing 210093, China. E-mail: xhxia@nju.edu.cn*
[b] *Department of Chemical Engineering, Loughborough University, Loughborough, Leicestershire, LE11 3TU, UK*
[c] *Department of Materials and Chemical Engineering, Pingxiang University, Pingxiang 337055, China. E-mail: lqrong2021@163.com*

† Electronic supplementary information (ESI) available: See DOI: 10.1039/c6cc08047b

(NG–Co) shows a high turnover frequency (TOF) of 2.53 s^{-1} at a relatively low overpotential of 0.40 V in 0.1 M KOH. To gain insight into the activity of NG–Co, we show that the counter anions of Co^{2+} ions have a certain impact on the coordination environments of Co^{2+} ions, leading to different electron donating/withdrawing strengths as reflected by the shift of the redox potentials of the $Co^{2+/3+}$ couple. A volcano behavior is observed where the OER activities occur as a function of the electron densities of Co^{2+} ions. The results emphasize the importance of a moderate electron density of catalytic sites in achieving high OER activity.

The NG precursor was synthesized by pyrolysis of a graphene oxide (GO)/melamine scaffold shaped in an ice template.[21] The obtained structure of NG has appropriate inner porosity at a mesoporous/microporous scale with a large surface area to facilitate mass transport. The N/O atoms within NG were assumed to have the ligand property due to their extra electrons compared to C atoms. Taking advantage of this feature, we tested the ability of NG to function as a potential support for various metal ions (M^{x+}), in order to generate electrocatalytic sites for the OER. Specific NG–M complexes were synthesized by mixing NG with M^{x+} (M^{x+} stands for Mn^{2+}, Fe^{2+}, Co^{2+}, Ni^{2+}, Cu^{2+} and Zn^{2+} ions that originated from MCl_2) in CH_3OH (Fig. 1a). Their electrocatalytic abilities toward the OER were characterized by current–potential polarization curves in 0.1 M KOH (Fig. S1, ESI†). Since the OER activity of the NG precursor was inert compared to the NG–M under the same conditions, we depicted an activity trend of NG–M by correlating the OER potentials with the d electron numbers of M^{x+} (Fig. 1b).[22,23] The result showed that the Co^{2+} containing electrocatalyst was superior to the others. Transmission electron microscopy (TEM) images indicated that the NG–Co sample remained as a graphene structure, and formation of metals and metal oxides was not observed (Fig. S2, ESI†). An X-ray photoelectron spectroscopy (XPS) survey showed that the electron density of Co^{2+} ions appeared to be lower upon coordination, as inferred from the positive shift of the binding energies of Co $2p_{3/2}$ and $2p_{1/2}$ by *ca.* 0.5 eV (Fig. 1c). This phenomenon reflected the stronger electron withdrawing ability of graphene due to the conjugated π-electrons. Meanwhile, the N 1s electrons in NG–Co exhibited higher energetic levels compared to that in NG, suggesting the occurrence of the electron donating effect from N atoms to Co^{2+} ions (Fig. S3, ESI†). The cyclic voltammograms (CVs) of NG–Co coated on a glassy carbon electrode (GCE) showed a pair of well-defined current peaks that were assigned to the redox of the Co^{2+}/Co^{3+} couple.[24–26] Both the oxidation and reduction currents increased linearly with the scan rate, demonstrating the surface confined states of Co^{2+}/Co^{3+} ions (Fig. 1d). From atomic absorption spectroscopic (AAS) measurements, the Co content of NG–Co was quantified to be $\sim 5.3 \times 10^{-7}$ mol mg^{-1}.

The OER polarization curves of NG–Co measured in 0.1 M KOH aqueous solution using rotating ring-disk electrodes (RRDEs, GC as the disk and Pt as the ring) are presented in Fig. 2a. Each electrocatalyst cast onto the GC disk electrode was at a mass loading of $\sim$24 μg cm^{-2}. The rotation speed of the RRDE during the measurements was kept at 1600 rpm to eliminate bubble accumulation. A significant anodic current appeared on NG–Co/GC starting at *ca.* 1.5 V *vs.* RHE. To investigate the OER activity of NG–Co, CVs of NG–Co/GCE were collected in non-aqueous CH_3CN electrolyte, which showed featureless capacitance (Fig. 2b). Addition of KOH aqueous solution (1/6, V/V) to the CH_3CN electrolyte resulted in an apparent anodic wave peaked at 0.51 V *vs.* Ag/Ag^+ (10 mM $AgNO_3$). In the RRDE results, the anodic current may contain some OER events electrocatalyzed by the NG matrix, or oxidation of carbon to CO_2. As observed from the polarization curve of NG (black curve, Fig. 2a), this part, however, can be trivial especially when the potential is lower than 1.8 V.

The intrinsic OER activity of NG–Co within the overpotential range from 0.3 to 0.5 V was assessed in terms of TOFs (defined as the number of OER events completed per electrocatalytic site per second, Fig. 2c).[27] Minimum TOFs were obtained when the

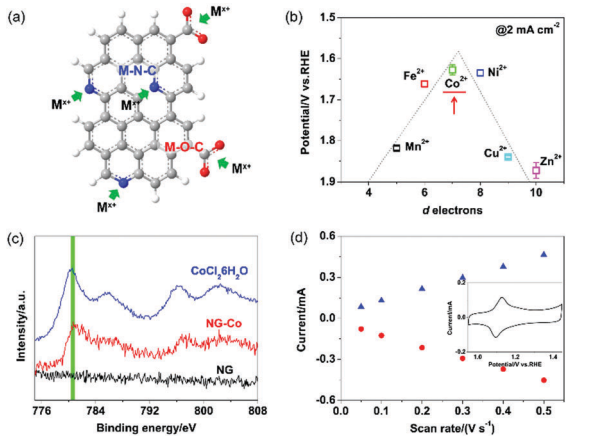

Fig. 1 (a) Proposed interacting mechanism between M^{x+} ions and NG. (b) OER potentials required at 2 mA cm^{-2} as a function of d electron numbers of transition metal ions (all potentials in the text are referenced to the reversible hydrogen electrode, RHE, if not specified). (c) XPS Co 2p surveys of $CoCl_2{\cdot}6H_2O$, NG and NG–Co. (d) Plot of the cathodic and anodic peak currents *versus* scan rates, the inset shows the CVs of NG–Co/GC, 0.1 M KOH, 50 mV s^{-1}.

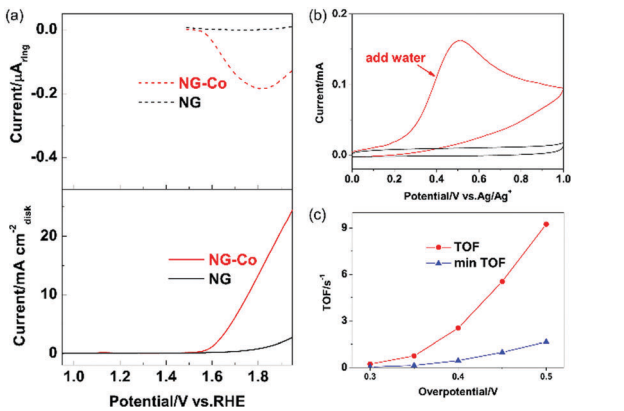

Fig. 2 (a) OER on NG–Co and NG in 0.1 M KOH, 10 mV s^{-1}, 1600 rpm. Ring current was recorded at 1.35 V. (b) CVs of NG–Co/GCE in CH_3CN with adding 0.1 M KOH (1/6 V/V), 50 mV s^{-1}. 0.1 M tetrabutylammonium perchlorate was applied as the electrolyte. (c) TOFs of the OER on NG–Co evaluated at overpotentials ranging from 0.30 to 0.50 V.

OER was assumed to occur on all the immobilized Co^{2+} ions of NG–Co/GC. The results showed that the TOFs became significant at overpotentials higher than 0.40 V (0.45 s^{-1}). In the electrocatalytic process, we believe that only Co^{2+} ions at the surface of NG–Co/GC actually are in contact with the electrolyte. The amount of Co^{2+} ions was therefore assessed by the charge for Co^{2+}/Co^{3+} redox in CVs, and the TOF significantly increased to 2.53 s^{-1}. This result surpasses those of many Co, Fe and Ni based catalysts reported recently (Table S1, ESI†). OER electrocatalysis on the NG–Co/GC electrode was continuously tested at 1.75 V for 6000 s. The NG–Co/GC retained more than 86% of its original anodic current. The corresponding TEM images show that the graphene structure of NG–Co was maintained without the formation of Co oxides after the measurements (Fig. S4, ESI†).

To demonstrate the contribution of Co^{2+} to the OER activity of NG–Co, vigorous acid treatment was performed to break the Co^{2+}–N/–O connections by protonation of N/O atoms. As expected, the XPS survey revealed that Co^{2+} detached from NG upon acid treatment, accompanied by an increase of overpotential for the OER by more than 150 mV and a substantial drop of electrocatalytic current (Fig. S5, ESI†). Besides, we found that the Co^{2+}–N sites may be more responsible for the OER activity. In another control experiment, graphene synthesized from pyrolysis of GO without melamine was used as a matrix to immobilize Co^{2+}. The GO derived graphene contained a certain amount of oxygen functional groups, such as carboxyl,[28] which could be the coordination sites to Co^{2+} ions. Using the same synthesis strategy, graphene was mixed with $CoCl_2{\cdot}6H_2O$ to form graphene–Co. Although the Co 2p signals in the XPS survey of graphene–Co were relatively ambiguous, the Co $2p_{3/2}$ peak could still be identified at a higher binding energy as compared to NG–Co. The electrochemical results showed that the graphene–Co also exhibited an improved activity toward the OER, although its catalytic activity was inferior to NG–Co as revealed by an onset potential difference of more than 100 mV (Fig. S6, ESI†).

In the RRDE measurements, the Pt ring was set at 1.35 V to probe the possible intermediates of the OER on NG–Co/GC. When the potential was scanned to 1.58 V, the Pt ring started to show a small cathodic current, which nearly disappeared on the NG or NG–Co treated with acid (Fig. 2a and Fig. S5c (ESI†), top graph). At such a high potential, the cathodic current most likely originated from the reduction of ROS intermediates, such as superoxide acid ($HO_2 + e \rightarrow HO_2^-$, $E^0 = 0.81$ V *vs.* NHE)[29] and hydroxyl radicals ($HO^\bullet + e \rightarrow HO^-$, $E^0 = 1.9$ V *vs.* NHE).[30] The latter would not be unreasonable when the OER was initiated from HO^- ions.[31] Our previous results have confirmed that the intermediate was $HO^\bullet$ by using a coumarin signal probe with an *in situ* fluorescence spectroelectrochemistry (Fig. 3a).[21,32] In 60 μM coumarin contained KOH solution, the OER on NG–Co was continuously performed at 1.65 V for 50 min. A fluorescence emission of the KOH electrolyte appeared at 500 nm (Fig. 3b), demonstrating the formation of 7-hydroxyl-coumarin. If HOO^- was involved in the OER, its decomposition might lead to the formation of $HO^\bullet$. This was not the case since addition of H_2O_2 to KOH electrolyte did not bring stronger fluorescence emission (Fig. S7, ESI†). Based on these results, it can be concluded that

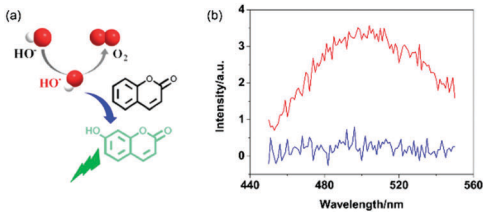

Fig. 3 (a) Conversion of coumarin into fluorescent 7-hydroxyl-coumarin by ROS formed in the OER. (b) *In situ* fluorescence spectroelectrochemistry of the OER performed at 1.65 V on NG–Co/GCE in 0.01 M KOH containing 60 μM coumarin for 50 min. The blue and red lines indicate the initial and final fluorescence emission of the electrolyte, respectively.

HO^- oxidation was initiated by the formation of $HO^\bullet$ *via* a 1e pathway (1),

$$HO^- \rightarrow HO^\bullet + e \quad (1)$$

Since $HO^\bullet$ is highly energetic, this step would require sufficient energy to improve the reaction kinetics, and thus be critical for the origin of the overpotential. On the other hand, it is worth pointing out that the NG–Co also exhibited an improved electrocatalytic activity toward the oxygen reduction reaction (ORR) as compared to that obtained from NG (Fig. S8, ESI†). By the *in situ* fluorescence spectroelectrochemistry, the ORR was also intermediated by the generation of $HO^\bullet$ (Fig. S9, ESI†). A faster reaction rate could be realized by lowering the activation energy barriers. Thus, the energy state of the highly energetic $HO^\bullet$ could affect both the overall pathways and kinetics of oxygen conversion.

Further centering on the Co^{2+} ions, their coordination states within NG–Co should be reasonably determined by the heteroatoms of NG as well as the nature of cobalt salt precursors. As seen in the energy dispersive X-ray spectroscopy images, both Co^{2+} and the Cl^- counter anions that originated from $CoCl_2{\cdot}6H_2O$ were identified to be distributed over carbon layers with close signal intensities (Fig. 4a). The Cl^- ions thus could be considered as liable ligands for Co^{2+} ions. Furthermore, by the

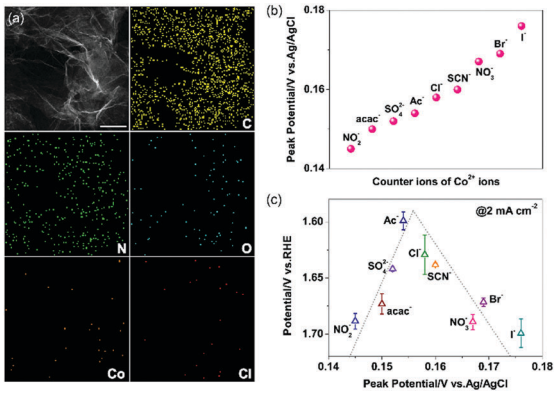

Fig. 4 (a) Elemental mapping images of NG–Co under HR-TEM characterization, scale bar: 500 nm. (b) DPV potentials of Co^{2+} ions on NG with different counter ions. (c) OER potentials required on NG–Co–L at 2 mA cm^{-2} as a function of the DPV potentials of Co^{2+} ions. Each symbol stands for the NG–Co–L synthesized from different cobalt salts.

same synthesis method as for NG–Co but using different cobalt salt precursors, we obtained a series of analogous Co^{2+} ion based electrocatalysts (NG–Co–L) with different counter anions (L = Ac^-, SCN^-, SO_4^-, NO_2^-, $acac^-$, NO_3^-, Br^- and I^- ions). Since the coordination states are determined by various factors, such as net charges, charge donating/accepting ability and numbers of ligands,[33] the exact natures of the ligands of NG–Co–L could be relatively complicated. To encompass all the possibilities for coordination results, we characterized the electron density of Co^{2+} ions to assess the impact from the natures of counter anions. This parameter was revealed by the redox potentials of Co^{2+} ions, which were obtained by differential pulse voltammetry (DPV) (Fig. S10 (ESI†), the DPV curve of NG was featureless under the same conditions).[34] The gradual increase of anodic peak potentials (E_{an}) indicates the stronger electron withdrawing effect occurring on Co^{2+} ions (Fig. 4b). The corresponding OER activities of NG–Co–L were then measured by the RRDE (Fig. S11, ESI†). It was found that the OER activities of NG–Co–L also varied with the counter anions. Optimum performance was observed on the electrocatalyst with median E_{an} values. Since the exact values of the onset potential of the OER can be somewhat ambiguous, we used the OER potential at 2 mA cm^{-2} as a parameter to evaluate the activities. As shown in Fig. 4c, a volcano like trend of the OER potential as a function of E_{an} of Co^{2+} ions appeared. If the OER potential was plotted at a lower current density of 1 mA cm^{-2} with respect to E_{an}, the volcano trend remained but with larger standard deviations (Fig. S12, ESI†). This volcano graph demonstrates that the electron density of Co^{2+} ions can be a general descriptor for OER activity. Since OER electrocatalysis at the heterogeneous interface was triggered by substrate chemisorption on active sites, electron density was generally governed by the bonding energy of chemisorption and thus determined the thermodynamics of the OER.[17] Besides, the influence of the coordination geometry of the active sites on the electrocatalytic activity of the NG–Co–L could not be a significant factor, as all these catalysts share a similar coordination geometry due to the rigid structure of NG.

We proposed and demonstrated a simple bottom up approach to the synthesis of heterogeneous Co^{2+} ion-nitrogen doped graphene complexes (NG–Co) under ambient environments. The as prepared NG–Co showed an excellent electrocatalytic activity toward the OER with a TOF of 2.53 s^{-1} at an overpotential of 0.40 V in 0.1 M KOH. Experimental results further demonstrated that the Co^{2+} ions encapsulated on NG could be fine tuned at the molecular level, *e.g.*, their electron densities in coordination structures were changed by using different counter anions. The derived activity trends exhibited a volcano-like shape, from which we concluded that the electron density of Co^{2+} ions could be one general activity descriptor to determine the overall electrocatalytic reaction. This work opens up a facile bottom up approach to the synthesis of highly active electrocatalysts and provides insights into the general catalyst design strategies.

This work was supported by the National Natural Science Foundation of China (21265016, 21327902, 21635004) and start-up funding from Loughborough University.

Notes and references

1 L. Schlapbach and A. Zuttel, *Nature*, 2001, **414**, 353–358.
2 M. G. Walter, E. L. Warren, J. R. McKone, S. W. Boettcher, Q. Mi, E. A. Santori and N. S. Lewis, *Chem. Rev.*, 2010, **110**, 6446–6473.
3 C. Liu, N. P. Dasgupta and P. Yang, *Chem. Mater.*, 2013, **26**, 415–422.
4 D. Gust, T. A. Moore and A. L. Moore, *Acc. Chem. Res.*, 2009, **42**, 1890–1898.
5 P. Yang and J.-M. Tarascon, *Nat. Mater.*, 2012, **11**, 560–563.
6 M. E. G. Lyons and M. P. Brandon, *J. Electroanal. Chem.*, 2010, **641**, 119–130.
7 D. E. Hall, *J. Electrochem. Soc.*, 1983, **130**, 317–321.
8 J. K. Nørskov, J. Rossmeisl, A. Logadottir, L. Lindqvist, J. R. Kitchin, T. Bligaard and H. Jónsson, *J. Phys. Chem. B*, 2004, **108**, 17886–17892.
9 C. C. L. McCrory, S. Jung, J. C. Peters and T. F. Jaramillo, *J. Am. Chem. Soc.*, 2013, **135**, 16977–16987.
10 M. Huynh, D. K. Bediako and D. G. Nocera, *J. Am. Chem. Soc.*, 2014, **136**, 6002–6010.
11 L. Trotochaud, J. K. Ranney, K. N. Williams and S. W. Boettcher, *J. Am. Chem. Soc.*, 2012, **134**, 17253–17261.
12 Y. Yang, H. Fei, G. Ruan, C. Xiang and J. M. Tour, *ACS Nano*, 2014, **8**, 9518–9523.
13 P. Ganesan, M. Prabu, J. Sanetuntikul and S. Shanmugam, *ACS Catal.*, 2015, **5**, 3625–3637.
14 H. Jin, J. Wang, D. Su, Z. Wei, Z. Pang and Y. Wang, *J. Am. Chem. Soc.*, 2015, **137**, 2688–2694.
15 M. S. Burke, L. J. Enman, A. S. Batchellor, S. Zou and S. W. Boettcher, *Chem. Mater.*, 2015, **27**, 7549–7558.
16 G. S. Hutchings, Y. Zhang, J. Li, B. T. Yonemoto, X. Zhou, K. Zhu and F. Jiao, *J. Am. Chem. Soc.*, 2015, **137**, 4223–4229.
17 J. Rossmeisl, Z. W. Qu, H. Zhu, G. J. Kroes and J. K. Nørskov, *J. Electroanal. Chem.*, 2007, **607**, 83–89.
18 Y. Umena, K. Kawakami, J. R. Shen and N. Kamiya, *Nature*, 2011, **473**, 55–60.
19 S. Bang, Y.-M. Lee, S. Hong, K.-B. Cho, Y. Nishida, M. S. Seo, R. Sarangi, S. Fukuzumi and W. Nam, *Nat. Chem.*, 2014, **6**, 934–940.
20 E. Y. Tsui, R. Tran, J. Yano and T. Agapie, *Nat. Chem.*, 2013, **5**, 293–299.
21 J. Wang, H.-S. Wang, K. Wang, F.-B. Wang and X.-H. Xia, *Sci. Rep.*, 2014, **4**, 6723.
22 J. Suntivich, K. J. May, H. A. Gasteiger, J. B. Goodenough and S. H. Yang, *Science*, 2011, **334**, 1383–1385.
23 J. Suntivich, H. A. Gasteiger, N. Yabuuchi, H. Nakanishi, J. B. Goodenough and Y. Shao-Horn, *Nat. Chem.*, 2011, **3**, 546–550.
24 P. Comba and A. F. Sickmüller, *Inorg. Chem.*, 1997, **36**, 4500–4507.
25 Y. Xie and T. W. Hamann, *J. Phys. Chem. Lett.*, 2013, **4**, 328–332.
26 S. M. Feldt, E. A. Gibson, E. Gabrielsson, L. Sun, G. Boschloo and A. Hagfeldt, *J. Am. Chem. Soc.*, 2010, **132**, 16714–16724.
27 A. J. Esswein, M. J. McMurdo, P. N. Ross, A. T. Bell and T. D. Tilley, *J. Phys. Chem. C*, 2009, **113**, 15068–15072.
28 W. Gao, L. B. Alemany, L. J. Ci and P. M. Ajayan, *Nat. Chem.*, 2009, **1**, 403–408.
29 P. Vanýsek, *Handbook of Chemistry and Physics*, 92nd edn, 2011.
30 J.-M. Noël, A. Latus, C. Lagrost, E. Volanschi and P. Hapiot, *J. Am. Chem. Soc.*, 2012, **134**, 2835–2841.
31 M. T. M. Koper, *J. Electroanal. Chem.*, 2011, **660**, 254–260.
32 J. Wang, K. Wang, F. B. Wang and X. H. Xia, *Nat. Commun.*, 2014, **5**, 5285.
33 T. Dudev and C. Lim, *Chem. Rev.*, 2014, **114**, 538–556.
34 M.-S. Liao and S. Scheiner, *J. Chem. Phys.*, 2002, **117**, 205–219.

Supporting Information

A Simple Way to Finely Tune the Redox Potentials of Cobalt Ions Encapsulated in Nitrogen Doped Graphene Molecular Catalysts for Oxygen Evolution Reaction

Jiong Wang[1], *Wen-Feng Lin*[2], *Yi Shi*[1], *Huai-Song Wang*[1], *Lian-Qing Rong*[3]* and *Xing-Hua Xia*[1]*

[1]State Key Laboratory of Analytical Chemistry for Life Science and Collaborative Innovation Center of Chemistry for Life Sciences, School of Chemistry and Chemical Engineering, Nanjing University, Nanjing 210093, China.
[2]Department of Chemical Engineering, Loughborough University, Loughborough, Leicestershire, LE11 3TU, U.K.
[3]Department of Materials and Chemical Engineering, Pingxiang University, Pingxiang 337055, China
E-mail: xhxia@nju.edu.cn (X.H. Xia) and lqrong2021@163.com (L. Q. Rong)

Experiments

Reagents and Apparatus. The Graphite precursor (99.9995%, 100 mesh) was purchased from Alfa Aesar Company. Metal chlorides, cobalt salts and other reagents were of analytical-reagent grade. All aqueous solutions were prepared using Millipore water with resistivity of 18.2 MΩ•cm. The morphologies of the prepared catalysts were characterized by transmission electron microscopy (TEM, JEM-2100, JEOL Company, Japan). The Raman spectra were carried out on a FT-Raman Spectrometer (Bruker Company, German). X-ray diffraction pattern was carried out on a X'TRA spectrometer (Switzerland). XPS survey were obtained on a PHI 5000 VersaProbe (UlVAC-PHI Company, Japan), and curve fitting of elemental fine spectra were performed using 20% Gaussian-Lorentzian peak shape. Atomic absorption spectroscopy was performed to measure the cobalt content in the catalysts (180-80 type, Hitachi Company, Japan).

Synthesis of Transition Metal Ions-Nitrogen Doped Graphene Catalysts. Graphite oxide (GO) was prepared according to the method reported previously. GO was mixed with melamine in aqueous solution at a mass ratio of 1: 10 (GO: Melamine). The resultant suspension was then quickly immersed into liquid nitrogen to grow ice crystal template, afterwards the hybrid was sublimated under vacuum below 0 ºC. The dried hybrid was annealed at 800 ºC in Ar atmosphere for 1 h to achieve nitrogen doped

graphene (NG). The NG was further mixed with different metal ions (chloride salts of Mn^{2+}, Fe^{2+}, Co^{2+}, Ni^{2+}, Zn^{2+} and Cu^{2+} ions) in CH_3OH at room temperature for 12 h, forming the final electrocatalysts (NG-M) which were further washed with EtOH for several times and then dried at room temperature. The electrocatalysts with different counter anions of Co^{2+} ions on NG (NG-Co-L) were synthesized by using the same methods as for NG-Co but by using different cobalt salts as precursors.

Electrochemical Measurements. Rotating ring disk electrode (RRDE, PINE Inc, USA) was applied to assess the OER and ORR performance on different catalysts. Typically, the disk (glassy carbon, 5.61 mm in diameter) was casted with 6 μL catalyst suspensions (1 mg mL^{-1}/ EtOH) as the working electrode, Ag/AgCl electrode and Pt wire were used as the reference and counter electrodes, respectively. The collection efficiencies (N) of each modified disk electrode was measured in 1 mM $Fe(CN)_6^{3+}$/0.1 M KCl electrolyte. The apparent electron number (*n*) of ORR was calculated in terms of the equation ($n = 4\ i_d / (i_d + i_r/N)$ as previously reported. The potentiostat used in this work was CHI 900D (CH Instrument Inc., USA). For electrocatalytic measurements of ORR and OER, the potentials *vs.* Ag/AgCl electrode were converted to the values referring to reversible hydrogen electrode (RHE). In 0.1 M KOH, the open circuit potential keeps at about 0.95 V (E(RHE) = E (Ag/AgCl) + 0.95 V).

TOFs of Co site was calculated in terms of the equation:

$$\mathrm{TOF} = (J \times A)/(4 \times F \times m),$$

where *J* stands for the anodic current density, *A* stands for the electrode surface area, *F* is Faraday constant (96485 C mol^{-1}) and *m* is the mole amount of Co^{2+} ions. For TOF calcuation, *m* was determined by the charge amount of $Co^{2+/3+}$ couple of CVs. For minimum TOF calculation, *m* was determined by the atomic absorption spectroscopy (AAS) measurement.

An in situ **Fluorescence Spectroelectrochemistry.** Using a typical three-electrode system, the electrocatalysis of OER and ORR on a GC electrode (3 mm in diameter) modified with 1 μL catalysts suspension in KOH was performed on a CHI 660D potentiostat (CH Instrument Inc., USA). A 60 μM signal probe of coumarin was added into the KOH electrolyte. The fluorescence variation was recorded on a RF-5301PC fluorescence spectrophotometer (Shimadzu, Japan) during OER and ORR. The concentration of KOH electrolyte was diluted to 0.01 M for avoiding hydrolysis of coumarin.[1]

Additional Results

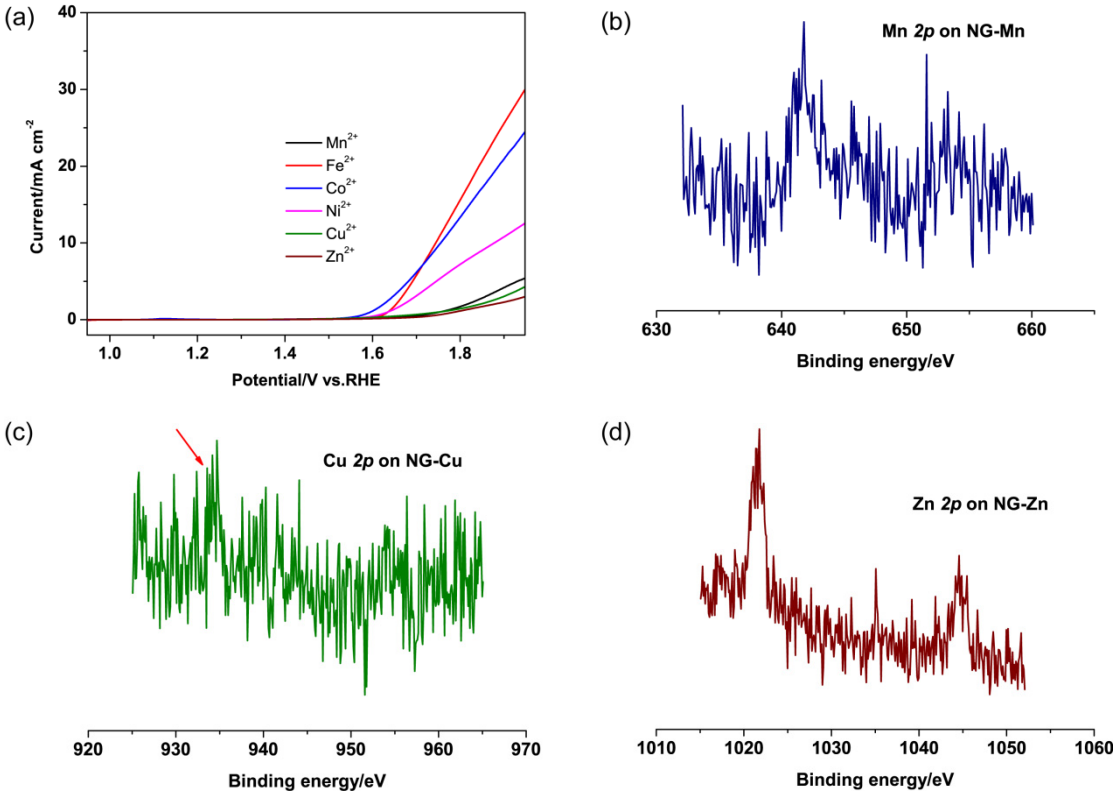

Figure S1. (a) OER polarization curves in 0.1 M KOH acquired on NG loaded with different ions: Mn^{2+}, Fe^{2+}, Co^{2+}, Ni^{2+}, Cu^{2+}, and Zn^{2+} ions, respectively. Rotation speed: 1600 rpm, scan rate: 10 mV s^{-1}. XPS spectra of Mn *2p* in NG-Mn (b), Cu *2p* in NG-Cu (c), and Zn *2p* in NG-Zn (d).

The electrocatalysts were synthesized using the same procedures, simply by mixing NG with the MCl_2 precursors (M= Mn, Fe, Co, Ni, Cu, and Zn). The NG-Mn, NG-Cu, and NG-Zn samples showed the lowest anodic currents. It could reflect that the loading efficiency of Mn^{2+} and Cu^{2+} ions was poor as indicated by the small XPS signals in Figure S1b and c. However, the Zn signal was relatively clear in the survey of NG-Zn (Figure S1d), which suggested that the intrinsic activity from Zn^{2+} ions was low. Therefore, another possible explanation for the inert OER activity can be that a filling state of *d* orbitals is a general descriptor describing the bond strength between active sites and HO^{-}. Too many (*e.g.*, Cu^{2+} and Zn^{2+} ions) or too few (*e.g.*, Mn^{2+} ions) *d* electrons would make the activation of substrate difficult by insufficient or overly strong chemisorption.[2]

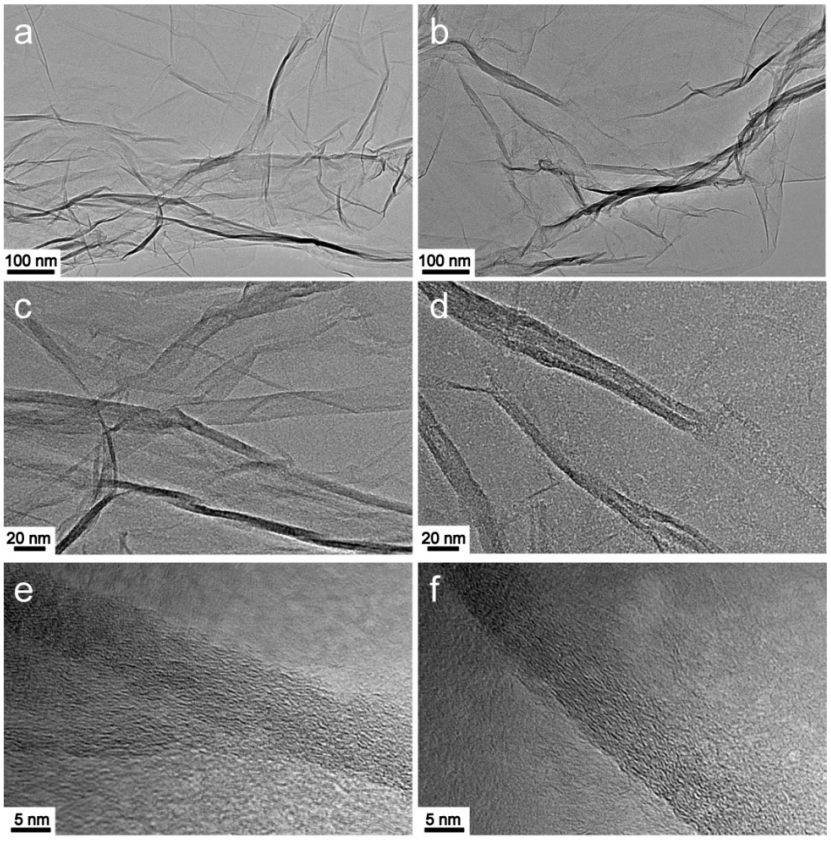

Figure S2. Typical TEM images obtained at different magnifications of NG before (a, c, e) and after (b, d, f) immobilizing Co^{2+} ions.

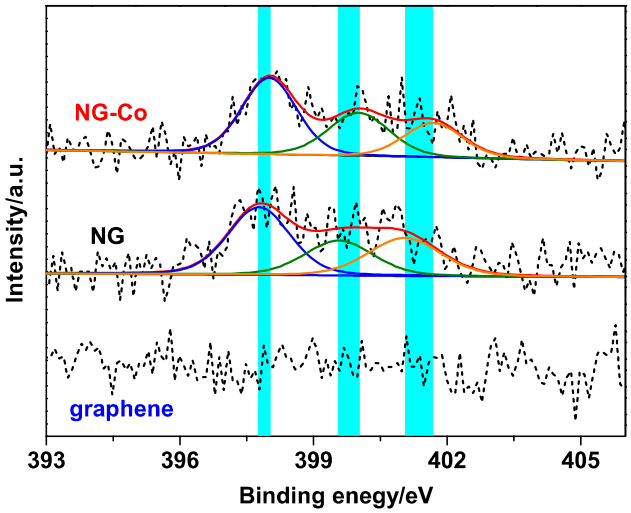

Figure S3. XPS survey of N *1s* electron levels in graphene, NG before and after immobilizing Co^{2+} ions.

Table S1. Several TOF values reported recently using different catalytic strategies.

Catalysts source	Electrolyte	Overpotential/V	TOF/s^{-1}
In this study	**0.1 M KOH**	**0.40**	**2.53**
ACS. Appl. Interfaces, **2014**, 5,10172	1 M KOH	0.30	0.0024
J. Am. Chem. Soc., **2013**, 135, 17242	0.1 M KOH	0.40 - 0.70	0.061-0.88
Nat. Commun., **2014**, 5, 4477	1 M KOH	0.30	0.05
J. Am. Chem. Soc., **2013***,* 135, 8452	1 M KOH	0.30	0.56
J. Am. Chem. Soc., **2010***,* 132 16501	0.1 M PBS	0.41	2×10^{-3}
Energy Environ. Sci., **2013**, 6, 2222	2 M KOH	0.60	2.9×10^{-4}
J. Am. Chem. Soc., **2013***,* 135, 4516	Na_2SiF_6 $NaHCO_3$	Photocatalysis	2.2×10^{-3}

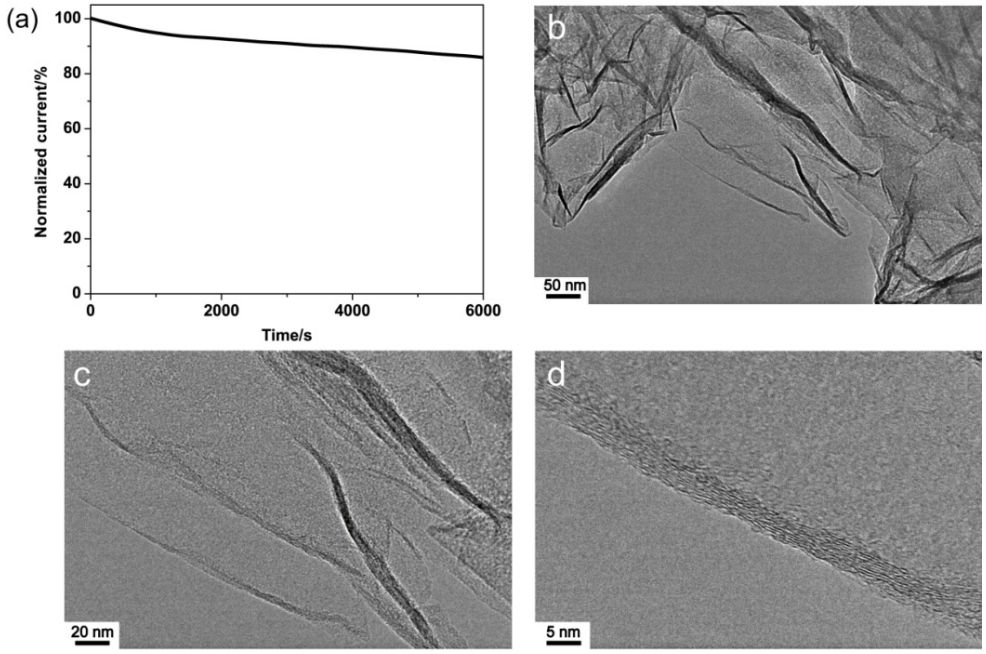

Figure S4. (a) Chronoamperometric response (normalized by the starting currents) of OER on NG-Co/GC in 0.1 M KOH at a rotation rate of 1600 rpm. The potential was set at 1.75 *vs.* RHE. (b, c, d) TEM images with different magnifications of NG-Co after the stability test.

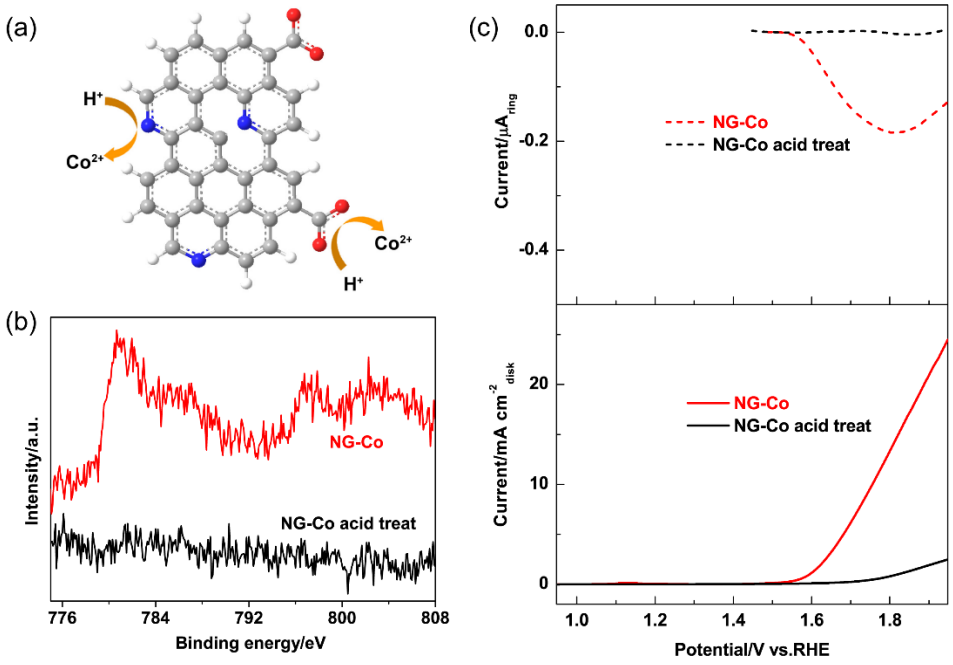

Figure S5. (a) Scheme illustrates the detachment of Co^{2+} ions from NG by acid treatment of NG-Co. (b) XPS survey of Co *2p* electrons of NG-Co before and after acid treatment. (c) OER polarization curves (bottom) and corresponding ring current (top) recorded at 1.35 V *vs.* RHE in 0.1 M KOH on Co-NG before and after acid treatment. Rotation speed: 1600 rpm, scan rate: 10 mV s^{-1}.

This control experiment was performed to verify the coordination interactions between Co^{2+} ions and NG. Briefly, prior to the test, the NG-Co was treated with 0.5 M H_2SO_4 at 80 ºC for 12 h to break Co^{2+}-N and/or Co^{2+}-O bonds. As a result, upon the detachment of active sites from NG, the degradation in OER current occurs. Meanwhile, the cathodic current on the Pt ring became difficult to identify.

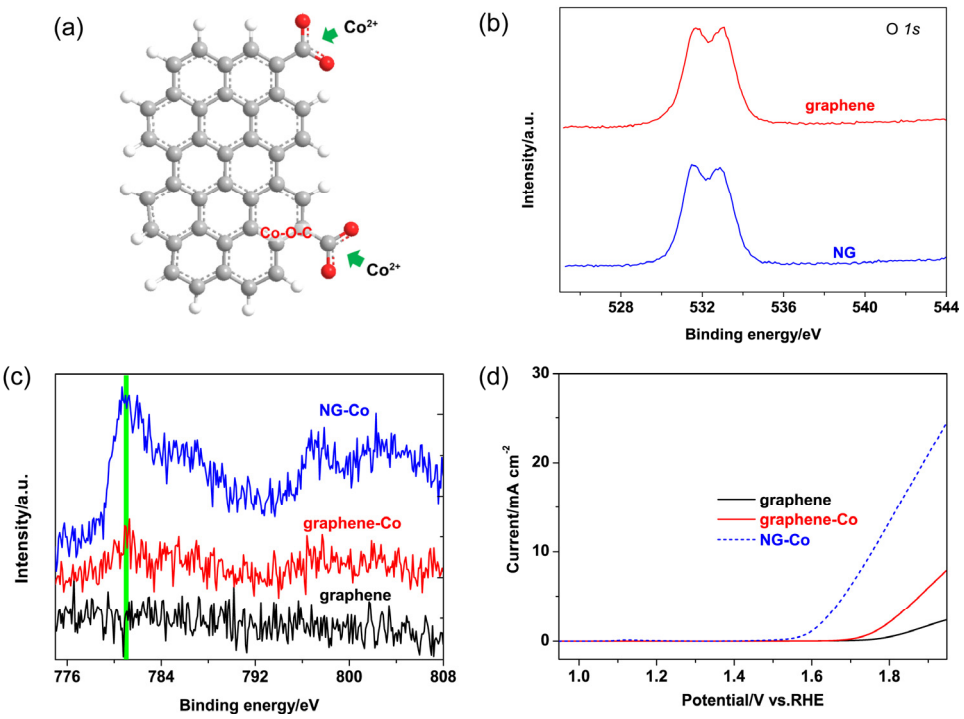

Figure S6. (a) Scheme indicates oxygen dopants in graphene driving the formation of graphene-Co. (b) O *1s* survey of NG and graphene. (c) Co *2p* surveys for graphene, graphene-Co and NG-Co. (d) Comparison of OER activities of graphene, graphene-Co and NG-Co in 0.1 M KOH. Rotation rate: 1600 rpm, scan rate: 10 mV s^{-1}.

Pyrolysis of GO in the absence of melamine resulted in the formation of graphene, which carries almost the same O-containing groups as in the NG case (Figure S6b). Using the same methodology to synthesize NG-Co, a control sample of graphene-Co was obtained by interacting graphene with Co^{2+} ions. However, weaker Co *2p* signals collected on the sample suggested that these O-containing groups had lower affinity to Co^{2+} ions comparing to the N dopants (Figure S6c). Although improvement of OER activity was observed on graphene-Co, it was not comparable to NG-Co as revealed by both overpotential and current density. These results implied that the N doping strategy can support more amount active sites within graphene, as well as leads to a more favorable adsorption for HO^{-} on Co-N.

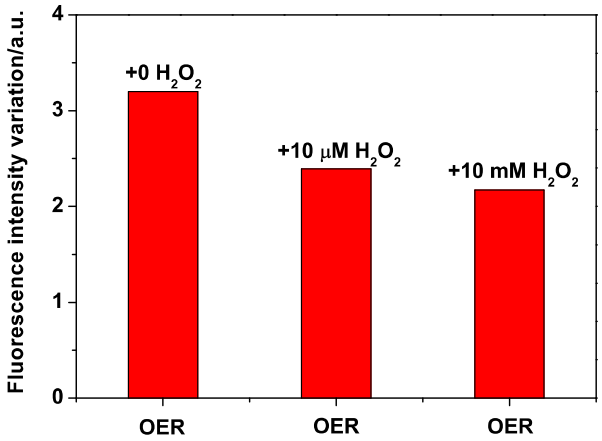

Figure S7. The fluorescence intensity variation from hydroxylation of coumarin during OER over NG-Co/GCE at 1.65 V *vs.* RHE for 50 min in 0.01 M KOH containing 0, 10 μM and 10 mM H_2O_2, respectively. The KOH solution was diluted to avoid hydrolysis of coumarin.

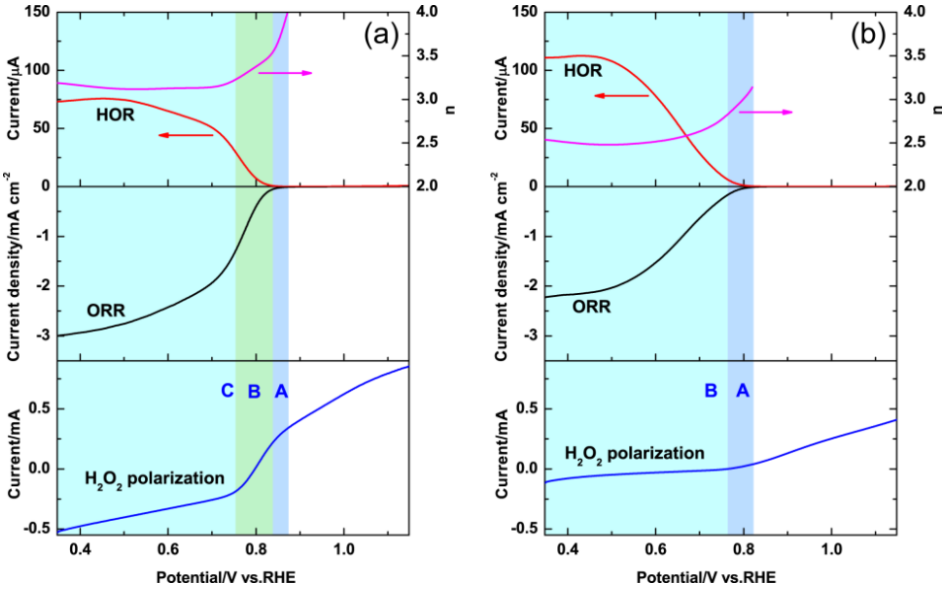

Figure S8. The ORR polarization curves acquired on NG-Co (a) and NG (b) in 0.1 M KOH, the corresponding H_2O_2 oxidation current on the Pt ring was recorded at 1.35 V and the derived *n* values were summarized. Rotation speed: 1600 rpm; Scan rate: 10 mV s^{-1}. Under the same conditions, the polarization of 6 mM H_2O_2 on NG and Co-NG was performed in 0.1 M KOH under N_2 atmosphere protection (bottom) at a rotation speed of 1600 rpm, and a scan rate of 10 mV s^{-1}.

The potentials lower than the standard potential of $E^{0'}(O_2/H_2O)$ were applied on the NG-Co/GC for evaluating the electrocatalytic activity for oxygen reduction reaction (ORR). In 0.1 M KOH, the polarization curves in RRDE measurements (Figure S8) showed that the NG-Co catalyst exhibited higher cathodic current with lower overpotential than NG, which demonstrated that the immobilized Co^{2+} ions also facilitated the *4e*-transfer ORR. Either direct or indirect *4e*-transfer reaction indicated that the electrocatalyst had the stronger capability to break O=O double bond as compared to *2e*-transfer of ORR. Within the potential range of ORR, the redox behavior of H_2O_2 on NG-Co and NG was compared. It can be seen clearly that NG-Co could effectively activate H_2O_2, showing a significant cathodic current as compared to the one obtained on NG. When certain amount of H_2O_2 was formed in the ORR on NG-Co, its redox contributed to the higher apparent electron transfer number (*n*) and cathodic current at the disk electrode.

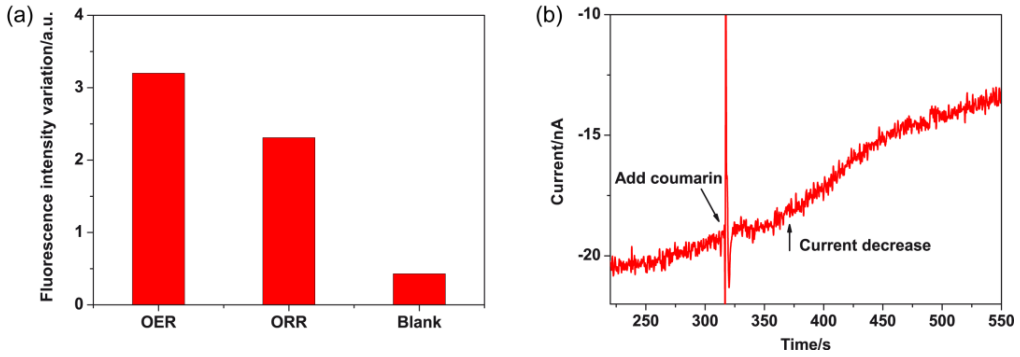

Figure S9. (a) Comparison of fluorescence emission after ORR and OER on NG-Co/GCE at 0.75 V *vs.* RHE and 1.65 V *vs.* RHE in 0.01 M KOH containing 60 μM coumarin for 50 min, respectively. The blank signal was obtained from a control experiment performed under the same conditions but without applying potential. (b) Current-time curve for ORR at 0.8 V *vs.* RHE in air saturated 0.01 M KOH (water/ethanol as solvent, 1:1 V/V). The ORR current jumped at 315 s which represented the injection of 0.6 mM coumarin into the electrolyte, afterwards it showed a gradual decrease.

As revealed by the *in situ* fluorescence spectroelectrochemistry measurements, the continuous running of ORR on NG-Co catalyst at 0.75 V *vs.* RHE also resulted in fluorescence emission at 500 nm, demonstrating the formation of fluorescent 7-hydroxyl-coumarin since there appeared only a relatively weaker fluorescence emission of the mixture of coumarin and KOH electrolyte at open circuit potential for the same time period (Figure S9a). Under ambient environments, the solubility of oxygen in KOH solution was relatively low (less than 10^{-3} M). It was observed that the cathodic current on NG-Co/GC gradually decreased in air-saturated KOH upon addition of more amount of coumarin (0.6 mM), which demonstrated the intermediate nature of $HO^{\bullet}$ in ORR (Figure S9b). Therefore, the process forming $HO^{\bullet}$ should be the main elemental step for 4e-transfer of ORR ($HO^{\bullet} + e \rightarrow HO^{-}$, $E^0 = 1.9$ V *vs.* NHE)[3], although the side pathway to generate HOO^{-} as byproduct could not be excluded.

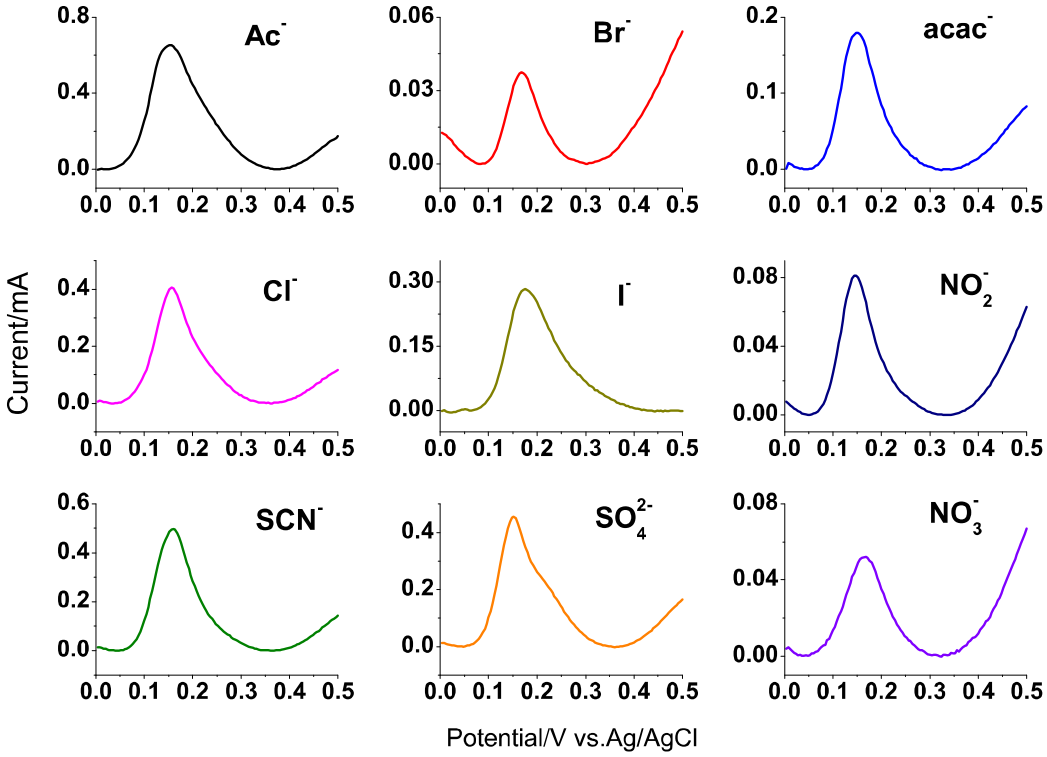

Figure S10. Differential pulse voltammograms (DPVs) of NG-Co-L prepared from cobalt salts with different counter anions. Amplitude: 50 mV; Pulse period: 0.2 s; Electrolyte: 0.1 M KOH. The Y-axis stands for the DPV current/mA and X-axis is potential *vs.* Ag/AgCl.

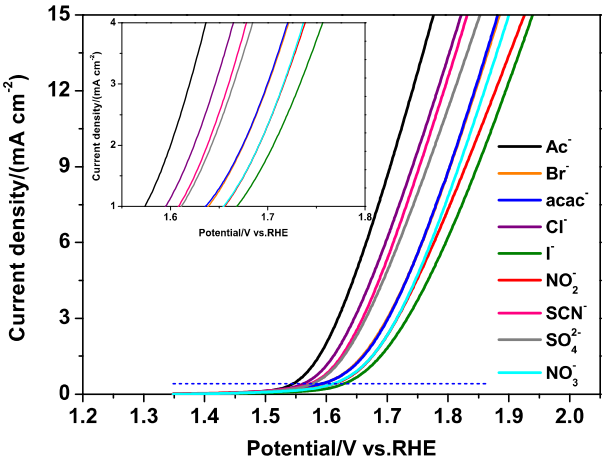

Figure S11. OER polarization curves obtained on NG-Co-L. Rotation speed: 1600 rpm, scan rate: 10 mV s^{-1}; Electrolyte: 0.1 M KOH.

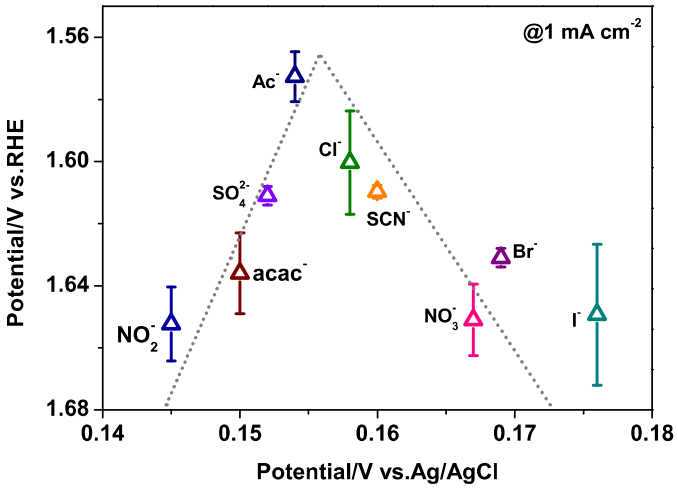

Figure S12. OER potentials required on NG-Co-L catalysts at 1 mA cm^{-2} as a function of anodic potentials of the immobilized Co^{2+} ions.

References

1. J. Wang, K. Wang, F.-B. Wang and X.-H. Xia, *Nat. Commun.*, 2014, 5.

2. J. Suntivich, K. J. May, H. A. Gasteiger, J. B. Goodenough and S. H. Yang, *Science*, 2011, 334, 1383-1385.

3. J. M. Noël, A. Latus, C. Lagrost, E. Volanschi and P. Hapiot, *J. Am. Chem. Soc.*, 2012, 134, 2835-2841.